Bioelectrochemistry 127 (2019) 163–170

Contents lists available at ScienceDirect

Bioelectrochemistry

journal homepage: www.elsevier.com/locate/bioelechem

A sensitive amperometric AChE-biosensor for organophosphate pesticides detection based on conjugated polymer and Ag-rGO-NH_2 nanocomposite

Pan Zhang [a,b], Tingting Sun [c], Shengzhong Rong [d], Dongdong Zeng [e], Hongwei Yu [a], Ze Zhang [a], Dong Chang [a,*], Hongzhi Pan [e,*]

[a] Department of Clinical Laboratory, Shanghai Pudong Hospital, Fudan University Pudong Medical Center, Pudong, Shanghai, China
[b] Public Health School, Harbin Medical University, Harbin, Heilongjiang Province, China
[c] Key Laboratory of Occupational Hazard Identification and Control, Public Health School, Wuhan University of Science and Technology, Wuhan, Hubei Province, China
[d] Public Health School, Mudanjiang Medical University, Mudanjiang, Heilongjiang Province, China
[e] Collaborative Research Center, Shanghai University of Medicine and Health Sciences, Pudong, Shanghai, China

ARTICLE INFO

Article history:
Received 11 September 2018
Received in revised form 4 February 2019
Accepted 4 February 2019
Available online 13 February 2019

Keywords:
Conjugated polymers
Amine functionalized reduced graphene oxide
Ag nanoparticles
Organophosphate pesticides
Acetylcholinesterase
Amperometric biosensor

ABSTRACT

Long-term accumulation of organophosphate pesticides in environment presents a potential hazard to human and animal health. Towards this, a highly sensitive amperometric AChE-biosensor based on conjugated polymer and Ag-rGO-NH_2 nanocomposite has been successfully developed. First, 4, 7-di (furan-2-yl) benzo thiadiazole (FBThF) was electrochemically polymerized on the electrode surface. Then, Ag-rGO-NH_2 nanocomposite and acetylcholinesterase (AChE) are modified on the polymer membrane surface. In this way, a novel amperometric AChE-biosensor was successfully prepared. The as-prepared biosensor possessed excellent conductivity, catalytic activity, and biocompatibility which were attributed to the synergistic effects of poly(FBThF) and Ag-rGO-NH_2 and provided a hydrophilic surface for AChE adhesion. Under optimized conductions, the linear range was 0.099–9.9 μg L^{-1} with a regression coefficient of 0.9947 for malathion, 0.0206–2.06 μg L^{-1} with a regression coefficient of 0.9969 for trichlorfon. The detection limit is calculated to be about 0.032 μg L^{-1} for malathion and 0.001 μg L^{-1} for trichlorfon (S/N = 3). Moreover, the biosensor exhibited acceptable reproducibility and long-term stability, which makes it possible to provide a novel and promising tool for analysis of organophosphate pesticides.

1. Introduction

Organophosphate pesticides (OPs) are widely utilized to improve agricultural productivity and control various insecticides in the worldwide. However, long-term accumulation in the environment presents a potential hazard to human and animal health [1–4]. The inhibition of acetylcholinesterase (AChE) activity by OPs can lead to a disturbance of normal neuronal function and death [5–7]. Hence, the reliable and rapid measurement of pesticides in water and food is of great significance. Recently, different analytical technologies and methods have been used to determine OPs, such as liquid chromatography–tandem mass spectrometry [8], high-performance liquid chromatography [9] and gas chromatography–tandem mass spectrometry [10]. In spite of their high sensitivity and reliability, these methods are limited to laboratory analysis currently, due to the high expense of experimental instrumentation and hard access to well-trained personnel, complicity of sample pretreatments and length of examining time [11,12]. Therefore, it is of great necessity to develop a simple and sensitive method for rapid detection of OPs.

Electrochemical biosensors have drawn people's wide attention since they boast their low cost, simple operation, on-site inspection, rapid response and excellent selectivity. Among them, AChE based electrochemical biosensors have received more and more attention for OPs determination due to their fast response, on-site analysis and high sensitivity and coupled with simple detectors were developed recently [13], in which the inhibition of enzyme activity is monitored by the change of oxidation current of thiocholine (TCh) upon a certain potential. The working mechanism based on acetylthiocholine chloride (ATCl) is shown as follows [13]:

$$\text{Acetylcholine chloride(ATCl)} + H_2O \overset{AChE}{\rightarrow} \textit{Thiocholine(TCh)} + \textit{Acetic acid} + Cl^- \quad (1)$$

$$2\text{Thiocholine} \rightarrow \textit{Dithio} - \textit{bis} - \textit{choline} + 2H^+ + 2e^- \quad (2)$$

* Corresponding authors.
E-mail addresses: dongchang1969@163.com (D. Chang), panhongzhilaoshi@163.com (H. Pan).

https://doi.org/10.1016/j.bioelechem.2019.02.003
1567-5394/

However, the amperometric AChE-biosensors for OPs detection suffer from loss of enzyme activity. And most importantly, the oxidation peak of thiocholine has a relatively high oxidation potential and its intensity is very weak, which lead to low sensitivity. So, there are mainly two approaches to improving the performance of the biosensors. One is to improve the efficiency of enzyme immobilization. Several methods are developed such as physical adsorption, electrostatic adsorption, covalent bonding, entrapment by means of sol–gels and cross-linking [14–16]. Among them, cross linking is more popular and a combination of covalent bonding and entrapment. Therefore, cross linking was selected in the present study. Moreover, we picked glutaraldehyde (GLA) as the cross-linking agent for the cross-linking between the aldehyde group of GLA and the amino group of the AChE, which not only provides high enzyme loadings, but also prevents the AChE from leaking from the electrode surface. However, most of the reported AChE electrochemical biosensors still face serious sensitivity problems. Therefore, we should pick appropriate conductive materials to solve the sensitivity problems. To modify electrodes with polymer and nanomaterials has been an effective strategy to reinforcing the catalysis strength and amplifying conductivity.

Conjugated polymers (CPs), one of polymer materials, are coined as "synthetic metals" and have attracted great research interests in various applications for its excellent conductivity [17]. CPs have been widely used in several applications such as solar cells, molecular electronics, electrochromic devices and biosensors [18–20]. The high conductivity of these materials can be attributed to the delocalization of π-bonded electrons over the polymeric backbone, which leads to some electronic properties, such as high electron affinities and low ionization potentials. CPs have homogeneous and manageable film character, reproducibility, stability, biocompatibility, easy production and efficient electron transfer ability, which make CPs a promising material of modified electrode [21].

Amine functionalized reduced graphene oxide (rGO-NH_2) as a new nano-modified material has attracted tremendous attention due to its extraordinary electrical conductivity, fast electron transfer kinetics, remarkable mechanical strength, large surface area and excellent biocompatibility [22]. These features make functionalized graphene a promising material for sensors and biosensors. However, the rGO-NH_2, when fabricated on smooth solid surfaces as a monolithic part, suffers from the drawbacks of low catalytic activity, resulting in the incomplete catalysis of ATCl and low current responce. Moreover, Ag nanoparticles (Ag NPs) have high conductivity, large surface area, biocompatibility and good catalytic activity [23]. Ag NPs have been used for hydrogen peroxide [24], cholesterol [25] and glucose [26] due to excellent catalytic activity. In addition, Ag NPs can provide a suitable microenvironment to maintain the bioactivity of biomolecules [27], promote more efficient electron transfer between the immobilized biomolecules and the electrode substrates. Therefore, Ag NPs can improve the analytical performance of biosensors.

n this study, we firstly prepared amperometric AChE-biosensor based on poly(FBThF) and Ag-rGO-NH_2 nanocomposite modified GCE to detect OPs. First, 4, 7-di (furan-2-yl) benzo [1,2,5] thiadiazole (FBThF) was electrochemically polymerized on the electrode surface. Then, Ag-rGO-NH_2 nanocomposite and AChE are modified on the polymer membrane surface. The poly(FBThF) and Ag-rGO-NH_2 nanocomposite possessed excellent conductivity, catalytic activity, and biocompatibility which could be attributed to the synergistic effects of poly(FBThF) and Ag-rGO-NH_2, thus providing a large and hydrophilic surface for AChE adhesion. Furthermore, glutaraldehyde as a crosslinking agent was used to immobilize AChE on the surface of poly(FBThF)/Ag-rGO-NH_2/GCE to keep efficient enzyme loadings. The biosensor exhibited high sensitivity, acceptable stability and reproducibility for the analysis of ATCl and pesticides. Scheme 1 described the working principle of the electrochemical amperometric AChE-biosensor based on poly (FBThF) and Ag-rGO-NH_2 nanocomposite.

2. Experimental

2.1. Materials

Acetylcholinesterase (AChE) (C3889-2KU), acetylthiochline chloride (ATCl), tetrabutylammonium hexafluorophosphate ($TBAPF_6$) and 2-(tributyl stannyl)furan were purchased from Sigma-Aldrich. 4,7-Dibromobenzo[c][1,2,5]thiadiazole, $PdCl_2(PPh_3)_2$, H_2O_2 (30%), hydrazine hydrate (85%), silver nitrate ($AgNO_3$), 3-aminopropyltriethoxysilane (APTES), glutaraldehyde (GLA), dichloromethane (DCM), acetonitrile (ACN) and tetrahydrofuran were purchased from Aladdin. Malathion and trichlorfon were obtained from AccuStandard. Graphite was purchased from Nanjing Ji Cang Nano Technology Co.Ltd.

2.2. Apparatus

Electrochemical measurements were conducted on CHI760E electrochemical workstation (Shanghai Chenhua, China) with a common three-electrode system, including GCE or the modified GCE as working electrode, Pt wire and Ag/AgCl as counter and reference electrode, respectively. Scanning electron microscopy (SEM) and transmission electron microscopy (TEM) were conducted on S-2150 (Hitachi High-Technologies Corp., Japan) and JEM-2100F(JEOL Ltd., Japan) respectively. X-ray diffraction (XRD) and fourier transform-infrared (FT-IR) were completed on D/max-2200/PC (Japan Rigaku Corporation) and Brukertensor 27 (Germany), respectively.

2.3. Synthesis of 4,7-Di(furan-2-yl)benzo[c][1,2,5]-thiadiazole

The 4,7-Di(furan-2-yl)benzo[c][1,2,5]thiadiazole was prepared according to the reported method with slightly modifications [18,28]. Briefly, a round-bottomed flask equipped with an argon inlet and magnetic stirrer was charged with 300 mg 4,7-Dibromobenzo[c][1,2,5] thiadiazole, 1.09 g tributyl(furan-2-yl) stannane and 25 mL tetrahydrofuran. The mixture was heated to reflux for 1 h under argon. Then, 71.6 mg $PdCl_2(PPh_3)_2$ was added to the mixture. Next, the mixture was heated to reflux under argon atmosphere for 2 days. Finally, the mixture was cooled to room temperature and the solid product was filtered off to give an orange solid that was washed with pentane and air-dried (yield: 79%).

2.4. Preparation of Ag-rGO-NH_2 catalyst

2.4.1. Preparation of GO

Graphene oxide (GO) was produced from graphite powder according to modified Hummers method [29–31]. 2 g graphite, 6 mL HNO_3 and 60 mL concentrated H_2SO_4 were added to a conical flask in an ice bath. The mixture was stirred for 2 h and then 8 g $KMnO_4$ was slowly added to the mixture within 20 min. The mixture was stirred at 45 °C for 1 h. Afterward, it was diluted with 350 mL of double distilled water. The reaction temperature was adjusted to 90 °C and the mixture was stirred for 30 min. Lastly, 8 mL H_2O_2 (30%) was added and mixed until a yellow color appeared. The yellow suspension was then centrifuged, and the obtained precipitate was washed with double distilled water until the pH of the filtrate was neutral and dried in vacuum at 60 °C.

2.4.2. Preparation of rGO

The preparation of reduced graphene oxide (rGO) was carried out by adding 2 g GO to 500 mL double distilled water with the aid of ultrasonic cleaner. Then, 20 mL hydrazine hydrate was added and the suspension was stirred for 2 days at 95 °C. Finally, the black solid was collected by centrifugation and washed with double distilled water for several times, and dried in vacuum at 60 °C overnight.

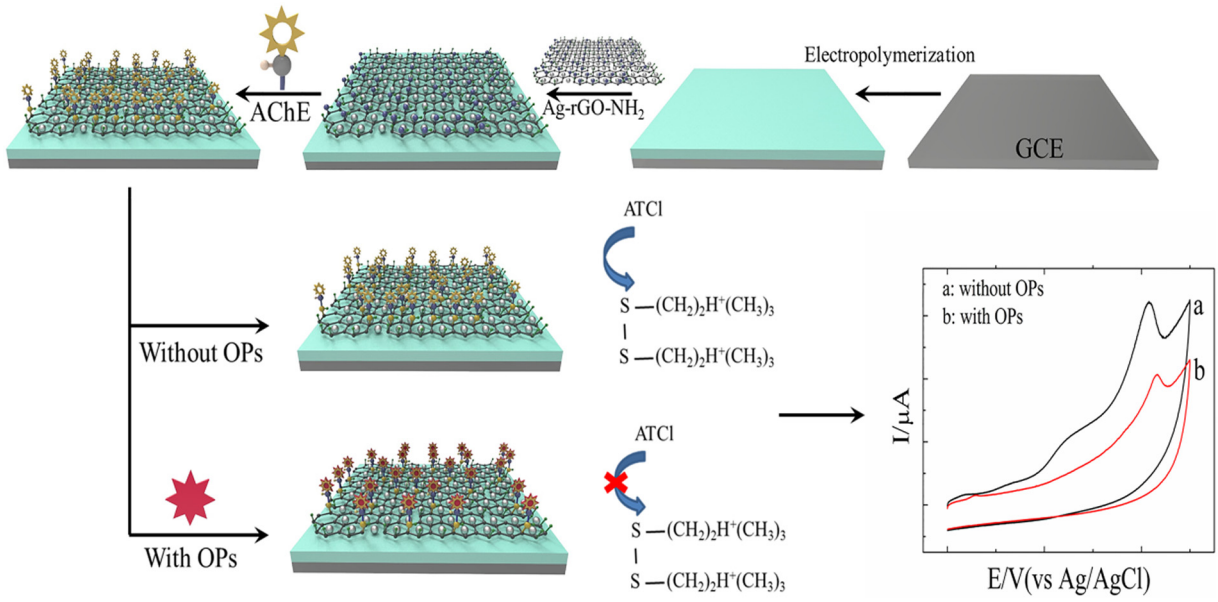

Scheme 1. Schematic representation of the preparation process for the proposed biosensor and the principle for OPs determination.

2.4.3. Preparation of rGO-NH_2

500 mg rGO was added to 30 mL toluene and stirred. Then, 5 g APTES was added to the suspension and stirred for 12 h. The prepared amine functionalized reduced graphene oxide (rGO-NH_2) was then collected by centrifugation and washed with toluene for several times, and finally dried in vacuum at 60 °C.

2.4.4. Preparation of Ag-rGO-NH_2

Preparation of Ag-rGO-NH_2 is as follows: First, 5.0 mg $AgNO_3$ was added to a conical flask containing 5 mL double distilled water and 100 mg rGO-NH_2. Then, 16 mg $NaBH_4$ was added and the mixture was stirred under air at room temperature for 1 h. After that, the precipitate was washed with double distilled water and methanol, respectively, and finally dried in vacuum at 150 °C.

2.5. Fabrication of biosensor

Prior to modification, the bare GCE was carefully polished to a mirror-like with 0.3 and 0.05 μm Al_2O_3 paste and sequentially sonicated in nitric acid ($v/v = 1:1$), ethanol and double distilled water respectively and dried with nitrogen. Subsequently, an electropolymerisation method was used to deposit poly(FBThF) film on the electrode while potential cycling was conducted by scanning the potential of the electrode between 0.0 and 1.4 V vs. Ag/AgCl at 100 mV s^{-1} for 55 cycles in $TBAPF_6$/DCM/ACN solution containing FBThF. After that, the electrode was washed with double distilled water and dried at room temperature. Then, 5 μL aqueous dispersion of the Ag-rGO-NH_2 (1 mg/mL) was dropped onto poly(FBThF)-coated surface and dried at room temperature. Then, 3 μL GLA (0.1%) and 10 μL AChE solution (100 U/mL) were dropped onto poly(FBThF)/Ag-rGO-NH_2/GCE and dried at 4 °C. The electrode was stored at 4 °C when not in use.

2.6. Measurement procedure

The suitability of the amperometric AChE-biosensor for work was checked by cyclic voltammetry (CV). Cyclic voltammograms were recorded prior to and after adding of 1 mM ATCl solution. The ATCl and pesticide concentrations were determined by CV. For the substrate detection, the biosensor was detected in 50 mM PBS (pH 7.5) containing different concentrations of ATCl solution. Then the current has been recorded until it had no longer changed. Concentration corresponding to the last shift of the current was then used as the substrate concentration. Before measurements, the AChE-biosensor was washed with 50 mM PBS (pH 7.5) three times to remove loosely adsorbed AChE.

For the measurements of pesticide, the sensing performance to pesticide was evaluated by recording CVs in 50 mM PBS (pH 7.5) containing 1 mM ATCl before and after incubating the electrode in different concentrations of OPs for 25 min. Then the signal towards ATCl was measured as described above. The inhibition percentage (I %) of pesticides to the enzyme electrode, which was taken as the sensing signal towards OPs, was got as following formula:

$$I\% = \frac{I_0 - I_1}{I_0} \quad (3)$$

where I_0 was the peak current of ATCl on the biosensor without OPs and I_1 was the peak current of ATCl on the biosensors with OPs inhibition.

3. Results and discussion

3.1. Characterizations of different nanocomposites

The surface morphologies of rGO-NH_2 and Ag-rGO-NH_2 nanocomposite were studied by SEM and TEM. As observed from Fig. 1a and c, the surface of rGO-NH_2 nanocomposite is covered with obvious ripples and wrinkles, which can increase the electrode surface area. For Ag-rGO-NH_2 nanocomposite (Fig. 1b and d), the Ag NPs are uniformly distributed on the surface of rGO-NH_2, which could be attributed to the "hot spots" and increase the electrocatalytic performance of the biosensor [32,33]. As shown in Fig. 1d, the size of Ag NPs is mostly about 15 nm, and a few are 50 nm and 75 nm. To determine the distribution of the Ag species, atomic-resolution high-angle-annular-dark-field scanning transmission electron microscopy (HAADFSTEM) measurement was conducted. The isolated bright dots of the first image in Fig. 1e can be unambiguously assigned to individual Ag atoms based on the *Z*-contrast difference between the heavier Ag and the other light atoms, clearly identifying the atomic dispersion of Ag anchored on rGO-NH_2 (Fig. 1e). Elemental mapping analysis of the STEM images revealed the homogeneous dispersion of Ag species in Ag-rGO-NH_2 (Fig. 1e). The sample nanocomposite was studied by energy dispersive X-ray spectroscopy (EDS) analysis (Fig. S1). The Ag peak was clearly

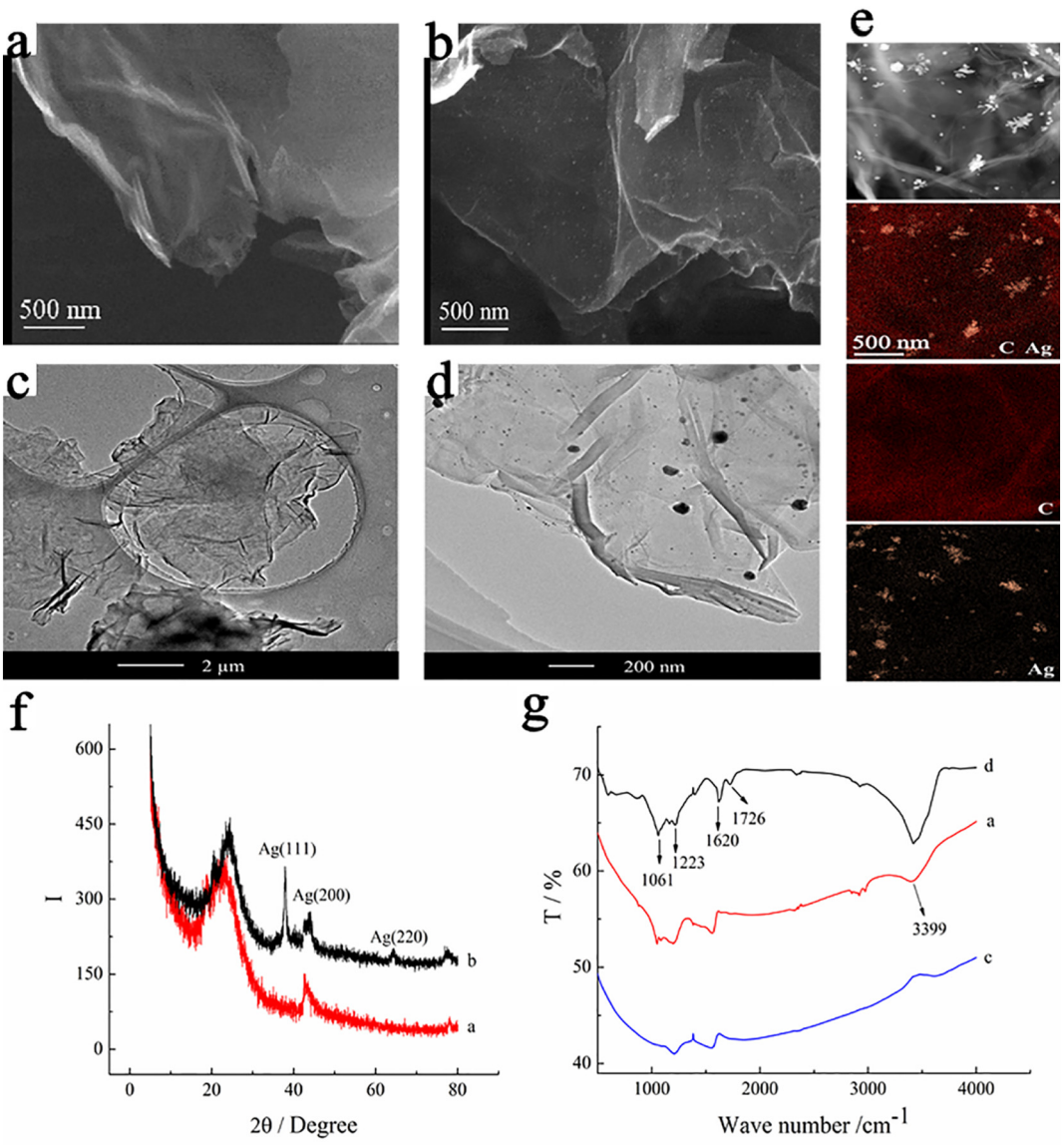

Fig. 1. SEM (a, b) and TEM (c, d) images of rGO-NH_2 (a, c) and Ag-rGO-NH_2 (b, d). HAADF-STEM image and elemental mapping of Ag-rGO-NH_2 (e). XRD patterns (f) of rGO-NH_2 (a) and Ag-rGO-NH_2 (b). FT-IR spectra (g) of rGO-NH_2 (a), rGO (c) and GO (d).

visible in the EDS spectrum, indicating that Ag has been successfully loaded on rGO-NH_2. Quantitative analysis of the EDS spectrum indicated that the atomic fraction of Ag loading on rGO-NH_2 is 0.71% (Fig. S1). Conclusively, the microscopy results provide solid evidence of the atomic dispersion of Ag species on the rGO-NH_2 support.

The XRD spectrum displayed a broad peak around $2\theta = 24°$ (Fig. 1 (f)) [34]. Meanwhile, in Fig. 1(f) curve b, the detected peaks observed at 38.1°,44.3°and 64°can be attributed to the (111), (200) and (220) planes of Ag nanoparticles according to Joint Committee on Powder Diffraction Standards (JCPDS) no. 01–087-0579.

In Fig. 1(g), the comparison of FT-IR spectra of GO and rGO-NH_2 reveals the great decrease in the intensity of characteristic absorption peaks of various oxygen-containing groups such as O—H, C═O and C—O, which supported the successful reduction of GO to rGO.

3.2. Characterizations of the electrode

SEM (Fig. S2) morphology of the poly(FBThF) reveled that cauliflower-like structure were distributed on the GCE surface, which could provide a large surface area and high loadings of enzyme.

Fig. 2(a) shows CVs of poly(FBThF)/GCE, poly(FBThF)/Ag-rGO-NH_2/GCE and poly(FBThF) / Ag-rGO-NH_2/AChE/GCE in 5 mM $Fe(CN)_6^{3-/4-}$ containing 0.1 M KCl at scan rate of 100 mV s^{-1}. As shown in Fig. 2(a), the background current of the poly(FBThF)/Ag-rGO-NH_2/GCE was much greater than it was for poly(FBThF)/GCE, indicating the former has a more highly accessible surface area and better conductivity. At the same time, the background current of the poly(FBThF)/Ag-rGO-NH_2/AChE/ GCE was the lowest in Fig. 2(a), which could be attributed to insulator properties of biomolecules hindering the transfer of electrons. This indirectly proves the satisfactory attachment of enzyme molecules.

As shown in Fig. 2(b), when ATCl was added, no certain peak was observed at poly(FBThF)/GCE, poly(FBThF)/Ag-rGO-NH_2/GCE. Meanwhile, the current at poly(FBThF)/Ag-rGO-NH_2/GCE was higher than that observed at poly(FBThF)/GCE, indicating that poly(FBThF)/Ag-rGO-NH_2/GCE improved the conductivity of the electrode. In addition, an irreversible peak was observed at poly(FBThF)/Ag-rGO-NH_2 /AChE/GCE and poly(FBThF)/AChE/GCE, which was coming from the hydrolysis product of ATCl catalyzed by AChE. Moreover, a big increase in the current was observed at poly(FBThF)/Ag-rGO-NH_2/AChE/GCE. There may be two

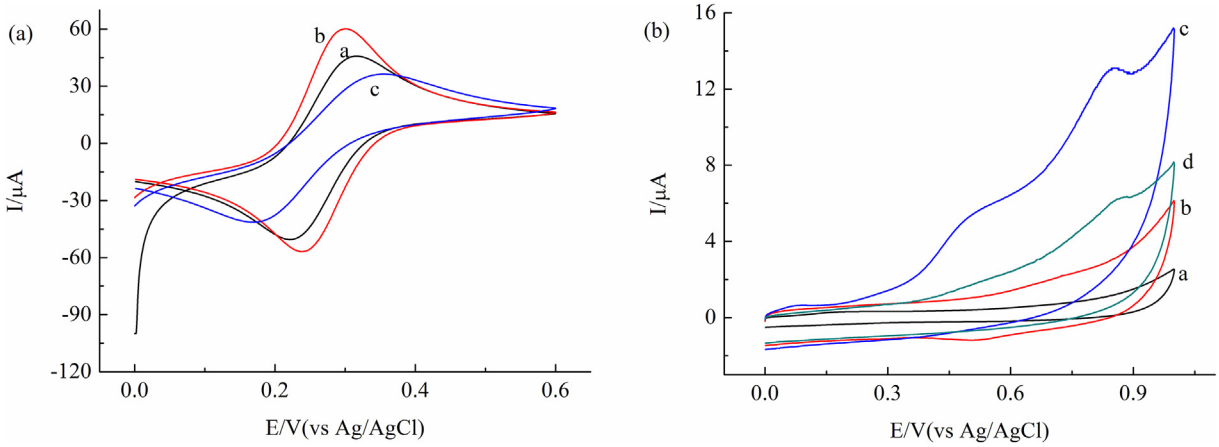

Fig. 2. (a) CVs of poly(FBThF)/GCE (a), poly(FBThF)/Ag-rGO-NH_2/GCE (b) and poly(FBThF)/ Ag-rGO-NH_2/AChE/GCE (c) in 5 mM $Fe(CN)_6^{3-/4-}$ containing 0.1 M KCl at scan rate 100 mV s^{-1}. (b) CVs of poly(FBThF)/GCE (a), poly(FBThF)/Ag-rGO-NH_2/GCE (b) and poly(FBThF)/ Ag-rGO-NH_2/AChE/GCE (c), poly(FBThF)/AChE/GCE (d) in 50 mM PBS (pH 7.5) containing 1 mM ATCl at scan rate 50 mV s^{-1}.

reasons: one was that the -NH_2 present on the Ag-rGO-NH_2 surface could bind with —COOH on the AChE surface through CO-NH bonding, which resulted in the catalytic activity of AChE immobilized on the poly (FBThF)/Ag-rGO-NH_2/AChE/GCE was superior to that of poly(FBThF)/ AChE/GCE. Another was that the Ag loaded on the surface of Ag-rGO-NH_2 exhibited excellent electrochemical activity for the oxidation of thiocholine by virtue of its unique catalytic activity.

3.3. Optimization of experimental parameters

Thickness of the polymer film on the electrode was studied using cyclic voltammetry. For this, several scan numbers were studied. As shown in Fig. 3(a), the highest response was recorded with 55-cycle deposition. If the film was too thick, diffusion problems between polymer coated transducer and biomolecules may arise resulting in a lower charge transfer rate. On the contrary, 3D structure of biomolecules on the very thin layer may not be satisfied causing a sort of denaturation. Furthermore, to achieve better biosensor performance, the amounts of Ag-rGO-NH_2 were optimized. As shown in Fig. 3(b), the current intensity increased with increasing the volume of Ag-rGO-NH_2 suspension (1.0 mg/mL) dropped on the GCE surface up to 5 μL, and significantly decreased with further increasing the volume of Ag-rGO-NH_2. The enhanced current intensity should be mainly attributed to an improved electrocatalytic performance of the Ag NPs and an increased AChE immobilization amount, which were resulted from the pleated nanostructure as probed by SEM. However, excessive composite nanomaterials could cause the thicker matrix layer, thus leading to low electrocatalytic activity, and slightly limiting the permeation of ATCl and OPs molecules through the immobilization matrix.

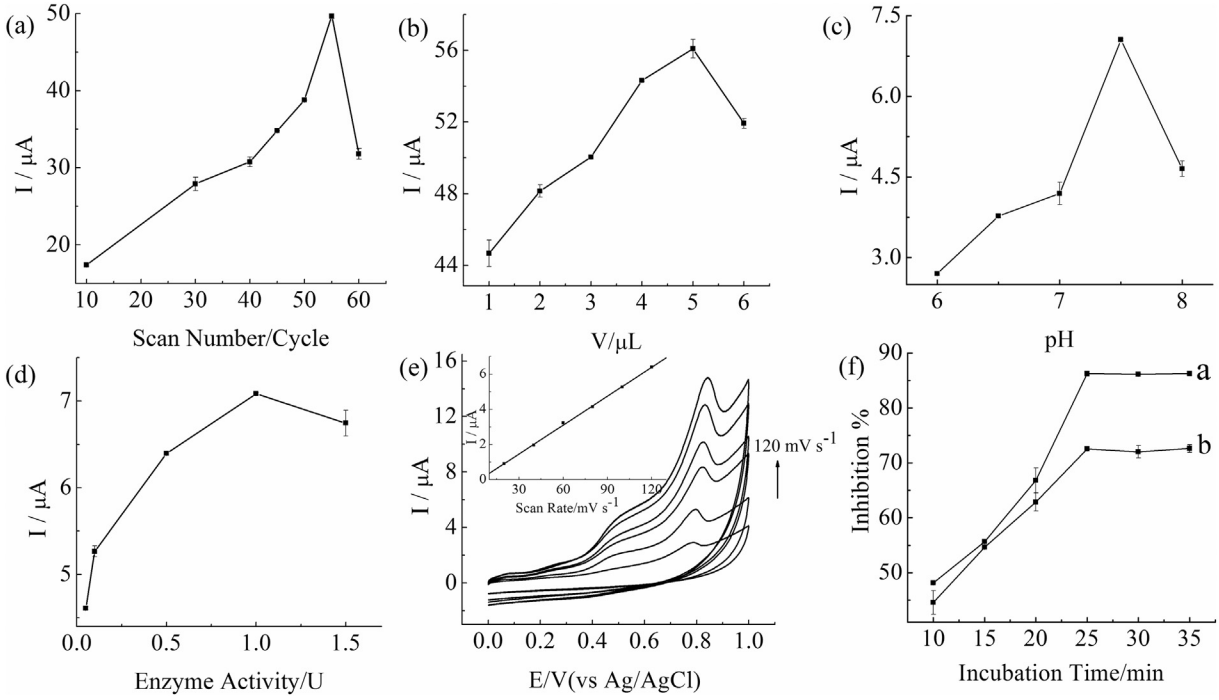

Fig. 3. (a) Effect of scan number, (b) Ag-rGO-NH_2 amounts, (c) pH (50 mM PBS at 6.0, 6.5, 7.0, 7.5, 8.0) and (d) enzyme activity (100 units of enzyme per unit volume of solution) on the biosensor response. (e) CV curves of poly(FBThF)/Ag-rGO-NH_2/AChE/GCE with 1 mM ATCl in 50 mM PBS (pH = 7.5) at different scan rate. The inset (e) is the calibration curves of current vs. scan rate ($I = 0.0548v - 0.1797$, $R^2 = 0.9989$). (f) Incubation time optimization for malathion (a) and trichlorfon (b). Error bars show standard deviation (SD) of three measurements.

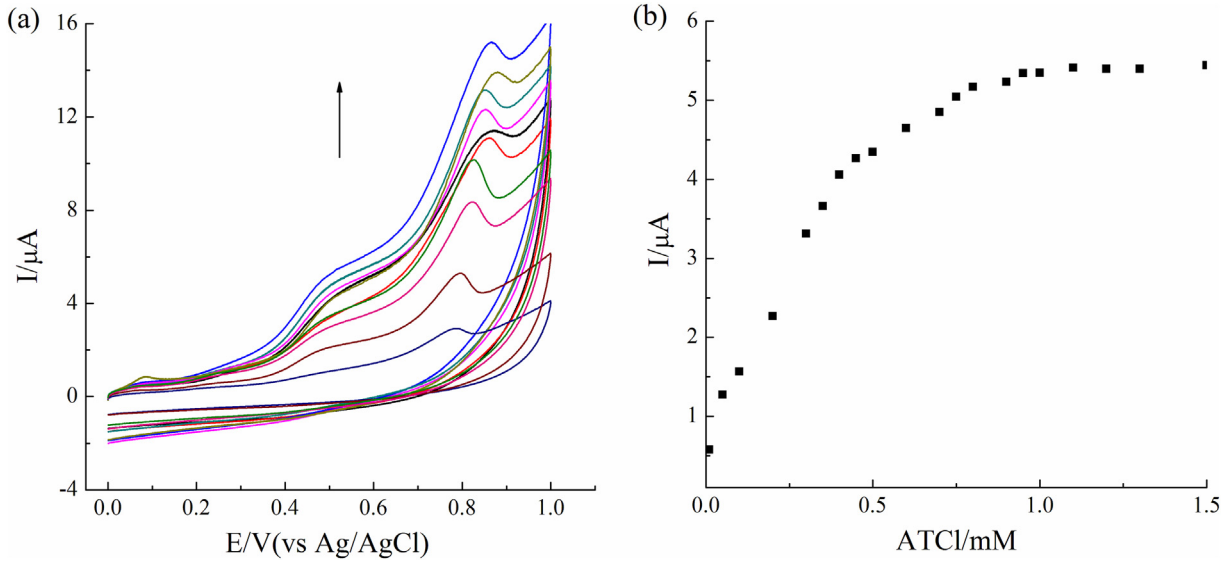

Fig. 4. CV curves of poly(FBThF)/Ag-rGO-NH_2/AChE/GCE with addition of ATCl to 50 mM PBS (pH = 7.5) at the scan rate of 100 mV s^{-1} (a) The calibration curve of current vs. concentrations of ATCl (b).

The activity of the immobilized AChE is proved to be dependent on the pH of phosphate buffer. Meanwhile, pH also has an effect on the degradation of ATCl. It may be due to the charged characteristics of the surface with pH and the interection of the charged surface and OPs during adsorption of OPs onto the poly(FBThF)/Ag-rGO-NH_2/AChE/GCE surface. The current response of the biosensor to 1 mM ATCl in the range of pH 6.0–8.0 (50 mM phosphate buffer) was studied. Fig. 3(c) showed that the maximum peak current was observed at pH 7.5. Therefore, pH 7.5 phosphate buffer was picked for subsequent experiments. The enzyme activity is one of among important aspects for biosensor. The effect of the enzyme activity ranging from 0.1 U to 1.5 U has been investigated in 50 mM PBS (pH 7.5) containing 1.0 mmol/L ATCl. From Fig. 3(d) it is obvious that the current responses increase with the increase of enzyme activity and reach the maximum at approximately 1.0 U, then decrease when the amount of enzyme activity is increased further. The decrease is probably owed to increasing diffusion limitation of AChE film's thickness.

To find out the mechanism of the reaction taken place on the poly (FBThF)/Ag-rGO-NH_2 / AChE/GCE, the kinetics of electrode reaction was studied by examining the influence of scan rate on the redox peak current. As shown in Fig. 3(e), the redox peak current (y = 0.0548x−0.1797, R^2 = 0.9989) increased linearly with the scan rate from 20 to 120 mV s^{-1}, which implies that the redox of ATCl on the poly(FBThF)/Ag-rGO-NH_2/AChE/GCE is an adsorption controlled process.

The inhibition time is one of the most important factors in the pesticide analysis. As shown in Fig. 3(f), each pesticide displays an increasing inhibition to AChE with the increase of immersion time, and when the incubation time is longer than 25 min, the curve trends to a stable value. So, 25 min was chosen as the incubation time for the detection of pesticide. The biosensor was immersed in 2-PAM for reactivation. It was shown that the biosensor inhibited by malathion could resume 89.94% of its original activity after reactivation. And the biosensor inhibited by trichlorfon could resume 90.80% of its original activity after reactivation.

The effect of ATCl concentration on the behavior of the AChE-biosensor was studied in 50 mM PBS (pH = 7.5). As shown in Fig. 4, the current response enhances rapidly with the increase of ATCl ranging

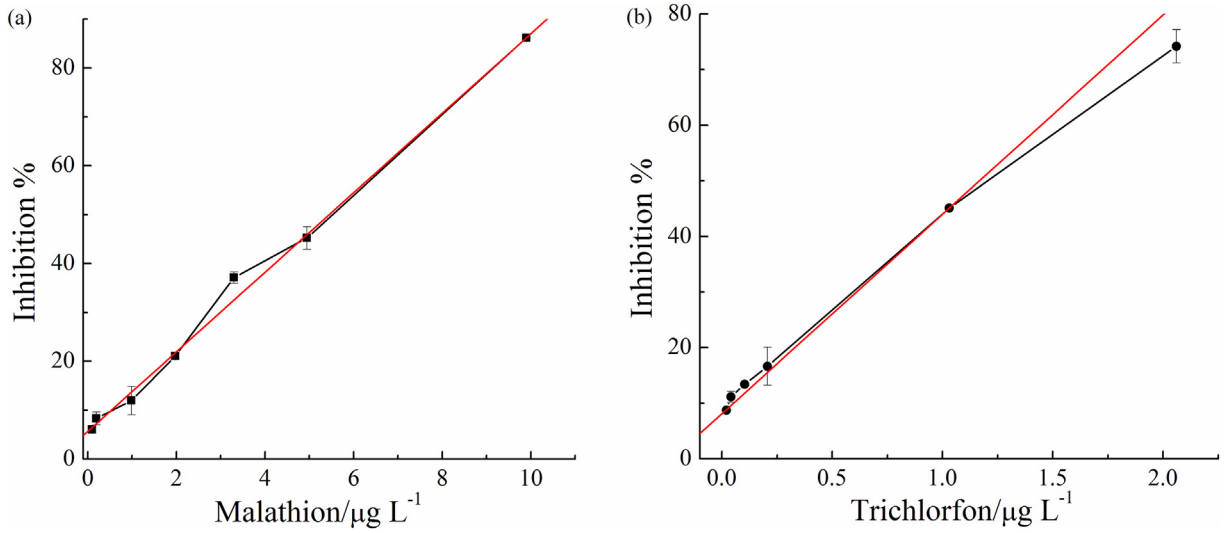

Fig. 5. Calibration curves for malathion (I% = 8.166 $c_{malathion}$ + 5.8627, R^2 = 0.9947) and trichlorfon (I% = 31.846 $c_{trichlorfon}$ + 9.8323, R^2 = 0.9969) (in 50 mM PBS, pH 7.5, 1.0 mM ATCl, 25 min of incubation time).

Table 1
Comparison of linear range and detection limit of AChE for malathion and trichlorfon with the present biosensor.

Pesticides	Modified electrode	Linear range (μg L^{-1})	LOD (μg L^{-1})	Ref
Malathion	poly(FBThF)/Ag-rGO-NH_2/AChE/GCE	0.099–9.9	0.032	This work
	Nafion/Ag-rGO-NH_2/AChE/GCE	6.3–77	4.5	[33]
	AuNPs/DAR/AChE/GCE	1.0×10^{-5} - 1.0×10^{-8}	5.12×10^{-9}	[35]
	HCS@PANI/AChE/GCE	1.0–10,000	0.16	[36]
Trichlorfon	poly(FBThF)/Ag-rGO-NH_2/AChE/GCE	0.0206–2.06	0.001	This work
	poly(FBThF)/f-MNPs/AChE	0.05–4.1 and 4.1–9	0.037	[18]
	AChE-PB/GCE	0.03–5	0.005	[37]

from 0.01 to 1.0 mM, and then the current response reaches saturation value. Meanwhile, the cyclic voltammograms of different concentrations of ATCl (from 0.01 to 1.5 mM) at the amperometric AChE-biosensor illustrated the Michelin-Menten process.

3.4. Detection of pesticides

Under the optimal conditions, the quantitative measurement of the prepared biosensor was investigated by incubating the different concentration of pesticides. As shown in Fig. 5, the linear range was 0.099–9.9 μg L^{-1} with a regression coefficient of 0.9947 for malathion, 0.0206–2.06 μg L^{-1} with a regression coefficient of 0.9969 for trichlorfon. The detection limit is calculated to be about 0.032 μg L^{-1} for malathion and 0.001 μg L^{-1} for trichlorfon (S/N = 3). The detection results of the poly(FBThF)/Ag-rGO-NH_2/AChE/GCE compared with previous reports were shown in Table 1. Also, the detection limit of this work is far below 50–100 μg L^{-1} of the Chinese national standard (GB13192–91), which is measured by Gas chromatography (GC). The prepared biosensor exhibited a wide linear range and lower detection.

3.5. Reproducibility and stability

The reproducibility of the proposed biosensor was determined by in PBS (50 mM PBS, pH 7.5) containing 1.0 mM ATCl using five electrodes after immersed in 1 μg L^{-1} of malathion and trichlorfon for 25 min. The RSD of malathion and trichlorfon was 2.30% and 3.44%, respectively, demonstrating that the proposed biosensor exhibited acceptable reproducibility.

The long-term storage stability is another important issue for practical application of the enzyme biosensor. When the enzyme biosensor was not in use, it was stored at 4 °C and measured daily, no obvious decrease in the response of ATCl was observed in the first 7-day storage. After a 30-day storage period, the biosensor can retain 82.7% of its initial current response, which indicated that the proposed biosensor exhibited acceptable stability.

3.6. Real sample analysis

To assess the reliability of the proposed biosensor, three replicates of tap water samples and apple samples at 3 different concentrations of malathion and trichlorfon were measured in this study, and the accuracy was estimated by the standard addition method. As shown in Table 2, the recovery rates ranged from 95.2% to 108.0% and the RSDs are lower than 5%, which indicates the proposed biosensor is a promising biosensor for the practical detection of malathion and trichlorfon.

Table 2
Recovery results of pesticides in real samples ($n = 3$).

Pesticides	Added (μg L^{-1})		Found (μg L^{-1})		Recovery (%)		RSD[a] (%)	
	Tap water	Apple	Tap water	Apple	Tap water	Apple	Tap water	Apple
Malathion	0.198		0.214	0.201	108.0	101.5	0.283	0.228
	0.99		0.978	0.989	98.8	99.9	0.778	0.659
	1.98		1.931	1.943	97.5	98.1	0.919	0.402
Trichlorfon	0.103		0.107	0.098	104.3	95.2	0.636	0.805
	0.206		0.204	0.207	99.2	100.2	0.417	0.439
	1.03		1.069	1.019	103.8	98.9	0.212	0.059

[a] RSD (%) calculated from three separate experiments.

4. Conclusions

In this study, we have successfully constructed one kind of amperometric AChE-biosensor based on poly(FBThF) and Ag-rGO-NH_2 nanocomposite for the determination of malathion and trichlorfon. The proposed biosensor system is sensitive to small substrate concentrations and very stable over time, with its activity remaining at a very high level even after 30 days of repeated measurements. It is anticipated that this system has potential applications in the simple, rapid and quantitative detection of OPs.

Acknowledgment

This study was financially supported by the National Natural Science Foundation of China (No. 81673229, 81703269, 81573200 and 81773480), Youth Innovation Promotion Association CAS (No.2017356), Important Weak Subject Construction Project of Pudong Health and Family Planning Commission of Shanghai (No.PWZbr2017-02) and Natural Science Foundation of Heilongjiang Province (No. QC2018120).

Appendix A. Supplementary data

Supplementary data to this article can be found online at https://doi.org/10.1016/j.bioelechem.2019.02.003.

References

[1] G. Aragay, F. Pino, A. Merkoci, Nanomaterials for sensing and destroying pesticides, Chem. Rev. 112 (2012) 5317–5338.
[2] J. Chang, H. Li, T. Hou, F. Li, Paper-based fluorescent sensor for rapid naked-eye detection of acetylcholinesterase activity and organophosphorus pesticides with high sensitivity and selectivity, Biosens. Bioelectron. 86 (2016) 971–977.
[3] M. Wei, S. Feng, Amperometric determination of organophosphate pesticides using a acetylcholinesterase based biosensor made from nitrogen-doped porous carbon deposited on a boron-doped diamond electrode, Microchim. Acta 184 (2017) 3461–3468.
[4] X. Liu, M. Song, T. Hou, F. Li, Label-free homogeneous electroanalytical platform for pesticide detection based on acetylcholinesterase-mediated DNA conformational switch integrated with rolling circle amplification, Acs Sensors 2 (2017) 562.
[5] D.M. QUINN, Acetylcholinesterase: enzyme structure, reaction dynamics, and virtual transition states, Chem. Rev. 207 (1987) 955–979.
[6] Y. Zhang, H. Liu, Z. Yang, S. Ji, J. Wang, P. Pang, L. Feng, H. Wang, Z. Wu, W. Yang, An acetylcholinesterase inhibition biosensor based on a reduced graphene oxide/silver nanocluster/chitosan nanocomposite for detection of organophosphorus pesticides, Anal. Methods 7 (2015) 6213–6219.
[7] M. Yang, H. Zhou, Y. Zhang, Z. Hu, N. Niu, C. Yu, Controlled synthesis of polydopamine: a new strategy for highly sensitive fluorescence turn-on detection of acetylcholinesterase activity, Microchim. Acta 185 (2018) 132.
[8] Y. Shin, J. Lee, J. Lee, J. Lee, E. Kim, K.-H. Liu, H.S. Lee, J.-H. Kim, Validation of a multiresidue analysis method for 379 pesticides in human serum using liquid chromatography–tandem mass spectrometry, J. Agric. Food Chem. 66 (2018) 3550–3560.
[9] X.L.L. He, H. Xie, C. Wang, X. Jiang, Lu K, Ionic liquid-based dispersive liquid–liquid microextraction followed high-performance liquid chromatography for the determination of organophosphorus pesticides in water sample, Anal. Chim. Acta 655 (2009) 52–59.

[10] C. Santos, D. Oppolzer, A. Gonçalves, M. Barroso, E. Gallardo, Determination of organophosphorous pesticides in blood using microextraction in packed sorbent and gas chromatography–tandem mass spectrometry, J. Anal. Toxicol. 42 (2018) 321–329.
[11] C.S. Pundir, N. Chauhan, Acetylcholinesterase inhibition-based biosensors for pesticide determination: a review, Anal. Biochem. 429 (2012) 19–31.
[12] M.B. Gumpu, N. Nesakumar, S. Nagarajan, S. Ramanujam, U.M. Krishnan, K.J. Babu, J.B. Rayappan, Design and development of acetylthiocholine electrochemical biosensor based on zinc oxide-cerium oxide nanohybrid modified platinum electrode, Bull. Environ. Contam. Toxicol. 98 (2017) 662–671.
[13] P.C. Abhilash, N. Singh, Pesticide use and application: an Indian scenario, J. Hazard. Mater. 165 (2009) 1–12.
[14] J.T.K.A. Joshi, R. Haddon, J. Wang, W. Chen, A disposable biosensor for organophosphorus nerve agents based on carbon nanotubes modified thick film strip electrode, Electroanalysis 17 (2005) 54–58.
[15] F.E.K.M. Kesika, J. Turana, M. Kolb, S. Timur, M. Bahadir, L. Toppare, An acetylcholinesterase biosensor based on a conducting polymer using multiwalled carbon nanotubes for amperometric detection of organophosphorous pesticides, Sensors Actuators B Chem. 205 (2014) 39–49.
[16] R.R. Dutta, P. Puzari, Amperometric biosensing of organophosphate and organocarbamate pesticides utilizing polypyrrole entrapped acetylcholinesterase electrode, Biosens. Bioelectron. 52 (2014) 166–172.
[17] H.A. Emine Guler, Guliz Bozokalfa, Bilal Demir, Gizem Oyman Eyrilmez, Murat Yavuz, Dilek Odaci Demirkol, T.E. Hakan Coskunol, Shuhei Yamada, Suna Timur, Yusuf Yagci, Bioapplications of polythiophene-g-polyphenylalanine-covered surfaces, Macromol. Chem. Phys. 216 (2015) 1868–1878.
[18] S.S.H. Dzudzevic Cancar, A novel acetylcholinesterase biosensor: core–shell magnetic nanoparticles incorporating a conjugated polymer for the detection of organophosphorus pesticides, ACS Appl. Mater. Interfaces 8 (2016) 8058–8067.
[19] P. Tyagi, Multilayer edge molecular electronics devices: a review, J. Mater. Chem. 21 (2011) 4733–4742.
[20] H. Chen, H. Zhang, R. Yuan, S. Chen, Novel double-potential electrochemiluminescence ratiometric strategy in enzyme-based inhibition biosensing for sensitive detection of organophosphorus pesticides, Anal. Chem. 89 (2017) 2823–2829.
[21] T.C. Gokoglan, S. Soylemez, M. Kesik, I.B. Dogru, O. Turel, R. Yuksel, H.E. Unalan, L. Toppare, A novel approach for the fabrication of a flexible glucose biosensor: the combination of vertically aligned CNTs and a conjugated polymer, Food Chem. 220 (2017) 299–305.
[22] D.N.K.J. Huang, J.Y. Sun, Z.W. Wu CH Han, Novel electrochemical sensor based on functionalized graphene for simultaneous determination of adenine and guanine in DNA, Colloids Surf. B 82 (2011) 543–549.
[23] R. Bala, S. Mittal, R.K. Sharma, N. Wangoo, A supersensitive silver nanoprobe based aptasensor for low cost detection of malathion residues in water and food samples, Spectrochim. Acta Part A 196 (2018) 268–273.
[24] F.L.W. Lu, Y. Luo, G. Chang, X. Sun, Hydrothermal synthesis of well-stable silver nanoparticles and their application for enzymeless hydrogen peroxide detection, Electrochim. Acta 56 (2011) 2295–2298.
[25] O.C. Siriwan Nantaphol, Weena Siangproh, Sensitive and selective electrochemical sensor using silver nanoparticles modified glassy carbon electrode for determination of cholesterol in bovine serum, Sensors Actuators B Chem. 207 (2015) 193–198.
[26] X.H.S. Chen, X.W. Chen, J.H. Wang, In situ growth of silver nanoparticles on graphene quantum dots for ultrasensitive colorimetric detection of H_2O_2 and glucose, Anal. Chem. 86 (2014) 6689–6694.
[27] Y.W. Liu, G. Li, C. Zhou, Q. Wang, M. Yang, L., a novel acetylcholinesterase biosensor based on carboxylic graphene coated with silver nanoparticles for pesticide detection, Mater. Sci. Eng. C Mater. Biol. Appl. 35 (2014) 253–258.
[28] J.Z. Yuan, J. Li, J. Lu, X. Huang, Z. Xu, W. Ma, Correlation between structure and photovoltaic performance of a series of furan bridged donor-acceptor conjugated polymers, J. Mater. Chem. A 1 (2013) 12128–12136.
[29] S. William Hummers, Richard E. Offeman, Preparation of graphitic oxide, J. Am. Chem. Soc. 88 (1958) 1339.
[30] Sasha Stankovich, Dmitriy A. Dikin, R.D. Piner, K.A. Kohlhaas, Synthesis of graphene-based nanosheets via chemical reduction of exfoliated graphite oxide, Carbon 45 (2007) 1558–1565.
[31] N. Syed, N. Alam, L. Sharma, S.N. Alam Kumar, Synthesis of Graphene oxide (GO) by modified hummers method and its thermal reduction to obtain reduced graphene oxide (rGO) * open access, Graphene (6) (2017) 1–18.
[32] C.R.S. Dutta, S. Sarkar, M. Pradhan, Y. Negishi, T. Pal, Silver nanoparticle decorated reduced graphene oxide (rGO) nanosheet: a platform for SERS based low-level detection of uranyl ion, ACS Appl. Mater. Interfaces 5 (2013) 8724–8732.
[33] V.T. Muhammet Guler, Zehra Basi, Determination of malation, methidathion, and chlorpyrifos ethyl pesticides using acetylcholinesterase biosensor based on Nafion/Ag-rGO-NH_2 nanocomposites, Electrochim. Acta 240 (2017) 129–135.
[34] S.G.J. Xu, F. He, N. Niu, P. Gao, Y. Chen, P. Yang, Reduced graphene oxide/$Ni_{1-x}Co_xAl$-layered double hydroxide composites: preparation and high supercapacitor performance, Dalton Trans. 43 (2014) 11667–11675.
[35] B. Jiang, P. Dong, J. Zheng, A novel amperometric biosensor based on covalently attached multilayer assemblies of gold nanoparticles, diazo-resins and acetylcholinesterase for the detection of organophosphorus pesticides, Talanta 183 (2018) 114–121.
[36] L. He, B. Cui, J. Liu, Y. Song, M. Wang, D. Peng, Z. Zhang, Novel electrochemical biosensor based on core-shell nanostructured composite of hollow carbon spheres and polyaniline for sensitively detecting malathion, Sensors Actuators B Chem. 258 (2018) 813–821.
[37] X.W.X. Sun, Acetylcholinesterase biosensor based on prussian blue-modified electrode for detecting organophosphorous pesticides, Biosens. Bioelectron. 25 (2010) 2611–2614.